

NONEQUILIBRIUM TRANSPORT IN NANOSCALE SEMICONDUCTOR DEVICES*

D. K. FERRY, S. M. RAMEY, L. SHIFREN AND I. KNEZEVIC
*Department of Electrical Engineering and Center for Solid State Electronics Research
Arizona State University
Tempe, AZ 85287-5706, USA
E-mail: ferry@asu.edu*

Soon, semiconductor devices will utilize very short gate lengths, of order 10-30 nm. These devices are expected to be dominated by quasi-ballistic, quantum transport in the active region. Simulation has developed as a major tool for predictive behavior of new devices, particularly with kinetic transport handled via a multi-particle Monte Carlo approach. Initial quantum effects have been incorporated into such simulations via an effective potential approach with great success, and we will discuss the application to small fully-depleted silicon-on-insulator devices. As devices grow smaller, however, more advanced techniques, such as the non-equilibrium Green's functions (NEGF) must be utilized, although there are constraints upon these approaches that must be incorporated into modeling of small devices. Nevertheless, approaches which derive from these NEGF structures, such as the Wigner distribution function, can still be implemented via the kinetic Monte Carlo approaches. The application of this approach to the modeling of a resonant tunneling diode also is discussed. The inclusion of both collisional broadening and the intra-collisional field effect into a Monte Carlo simulation of the Wigner function transport is described.

1. Introduction

As the density of integrated circuits continues to increase, there is a reduction in the dimensions of the devices of which they are comprised. Currently (2002), 0.07 μm is the state-of-the-art gate length in production, but smaller dimensions are expected in the near future. In addition, small semiconductor structures have been proposed for quantum computation with both the quantum wave and the spin as an appropriate information state. In all these devices, the transport is expected to be dominated by quantum effects, even though quantum transport for these small (and inhomogeneous) devices is not well established within a consistent conceptual framework [1]. Nevertheless, several approaches to simulation of some semiconductor devices have appeared in which the transport

* Based on a talk presented at the conference "progress in nonequilibrium green's functions, Dresden, Germany, 19-22 August 2002"

is handled quantum mechanically [2]. Of all the simulation methods currently employed, ensemble Monte Carlo (EMC) is the most robust method for device simulation, as it is proven to be reliable and predictive. Consequently, there is interest in studying how to incorporate quantum effects into this method.

In Boltzmann transport theory (BTT), processes are viewed on a coarse-grained time scale $t \gg \tau_{\text{coll}}$, where τ_{coll} is the *collision duration time*. In fact, BTT is more limited, as the time scale over which changes in the distribution function occur is required to be larger than any relevant relaxation times for momentum, energy, etc. In addition, each collision is treated as completed process prior to the next one, and is local in both space and time—e.g., there is no time duration to the scattering process, it occurs at a single point, and there is no multiple scattering—as well as being independent of any driving fields. It is often assumed that any deviation from these assumptions requires a quantum transport approach. In fact, coarse-grained time is a property of BTT itself, rather than of classical transport, as it neglects the convolution in the scattering integral that is important at short times. While this is certainly important in quantum transport, treatments can be expressed in classical transport [3]. Such non-Markovian behavior is intrinsic to EMC, and explicit in molecular dynamics. As a result, the factors that separate classical transport from a quantum treatment are the locality of the scattering and the non-interference of driving and relaxation forces. These effects are closely connected.

In BTT, the independence of the scattering events means that the energy is a well-defined function of the carrier momentum. If we define the carrier energy as $E = \hbar\omega$, and the momentum is defined through a function $E_{\mathbf{k}}(\mathbf{k})$, then semi-classical treatments assume that the spectral density function (the relation between ω and \mathbf{k}) is given by

$$A(k, \omega) = \delta(\hbar\omega - E_{\mathbf{k}}). \quad (1)$$

Here, the energy is defined only *on the shell* determined by $E_{\mathbf{k}}$. The most common breakdown occurs in heavily-doped systems, where the electron (or hole) density is high. The many-body interactions among the carriers lead to a renormalization of the energy bands (referred to as “band-gap narrowing” in the semiconductor device world) and *dressing* of each particle leads to a change in the effective mass. The spectral density $A(k, \omega)$ is no longer defined by Eq. (1). As a result, the energy is no longer easily connected to the function $E_{\mathbf{k}}$, and *off-shell* contributions are made in each of the important interactions. In near equilibrium situations, quantum transport may be handled through Green’s functions, either the zero-temperature Green’s functions used for low temperatures, or the thermal Green’s functions used for thermal-equilibrium systems. Perhaps the most important goal of these treatments is the

determination of the spectral density and the modified density-of-states function that results from it. However, neither of these approaches are suitable for the far-from-equilibrium transport that occurs in semiconductor devices. Although non-equilibrium (real time) Green's functions (NEGF) have been suggested for this, this approach has not addressed the issue of the non-locality of the scattering [4].

The non-locality of the scattering processes arises due to the fact that the collision actually requires a non-zero amount of time to complete. This is different from the non-locality of quantum mechanics itself. Here, the scattering process has an interaction volume and a collision duration time, both of which violate the assumptions of BTT. These effects also allow for multiple collisions to occur simultaneously, and carrier-carrier, and carrier-impurity scattering can be treated through a real-space Coulomb interaction within the ensemble Monte Carlo approach. These easily incorporate this multiple scattering effect [5,6]. However, the inclusion of the collision duration time, and the non-locality of the scattering, is a fully quantum mechanical effect, although attempts have been made to include them in some ensemble Monte Carlo techniques [7].

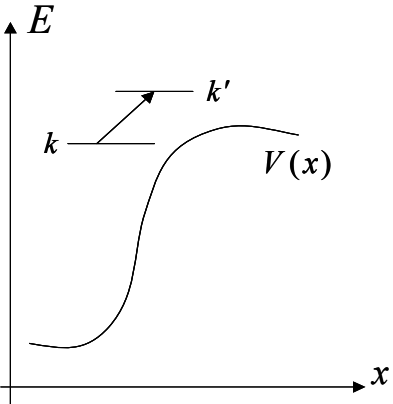


FIG. 1. Conceptual picture of an electron absorbing a phonon near a potential barrier.

Why this becomes important can be understood by consideration of Fig. 1, where we show an initial and final state of a phonon absorption process in the presence of a very inhomogeneous conduction band edge—just the type of conduction band edge that one finds in a typical device. Here, a particle approaches a potential barrier and absorbs a phonon near the barrier. Classically, the transition indicated in Fig. 1 is forbidden, as it is non-local in space. Absorbing a phonon normally leads to an *increase* in the momentum wave vector, but here the final state has a *lower* value of momentum wave

vector due to the increase in the potential energy. The horizontal lines are meant to estimate the spatial extent of the wave packets. The energy that is conserved is the *total* energy, not just the kinetic energy. In Fig. 1, it is the *intra-collisional field effect* [8] which rapidly changes the momenta of the two states with position (time).

So far, nothing has been said about the size quantization of a device structure, which itself is thought to introduce a need for quantum transport. The effect of this size quantization on the density response to a bias change is an important effect in devices, and is perhaps the first quantum effect that is important to consider, even though it does not require a full quantum transport treatment. In some sense, the size quantization is a problem, in which one must begin to worry about the effective size of the carriers themselves [9]. As we will see in the next section, it is this latter concern that leads to an effective potential which allows for the consideration of size quantization in a semi-classical Monte Carlo transport treatment of the device. Following this, we turn to a Wigner transport picture, but with a Monte Carlo that is modified to account for phase interference and the non-locality of quantum mechanics itself, and which incorporates the non-locality of scattering into a Monte Carlo transport treatment. Finally, we discuss some residual problems of general quantum transport that become quite important for small semiconductor structures.

2. The Effective Potential

Quantum confinement is known to occur in the channel of MOSFETs in the direction normal to the oxide interface. For quite some time, there has been a desire to categorize this quantization and determine the role it plays in semiconductor devices. This may be found by solving the Schrödinger and Poisson equations to find the charge and the changes in mobility and capacitance [10], but this is often too difficult to repeat often in the device simulation. More recently, a *quantum potential* was included as a correction to the self-consistent solutions of the Poisson equation [11]. This latter approach is called the “density-gradient” approach, since the quantum potential is defined in terms of the local density. We follow a different approach, which introduces an *effective* potential. Here, the natural size of an electron wave packet is used to introduce a smoothing of the local potential (found from Poisson’s equation) [12]. This approach naturally incorporates the quantum potential, which is an *approximation* to the effective potential. The effective potential follows two trends that have been prominent in statistical physics during most of the twentieth century (and into the current century). These are the non-zero size of

an electron wave packet and the use of a modified potential to describe quantum effects within classical statistical mechanics.

2.1 Defining the Effective Potential

The wave packet in real space includes contributions from all occupied plane wave states [9]. That is, the states that exist in momentum space are the Fourier components of the real-space wave packet. Hence, the phase space is important. There have been a number of studies of the manifestation of classical phase-space structure in quantum systems [13]. These have shown that meaningful, sharp structure can exist in quantum phase-space representations, and can be used to explain quantum dynamics; e.g. to study the quantum effects that arise in otherwise classical simulations. The use of a Gaussian wave packet as a representation of the classical particle is the most common basis (the well-known coherent-state representation). Here, the phase-space representation of the quantum density localized at point \mathbf{x} is given by [14-16]

$$\langle \mathbf{x} | \mathbf{p}, \mathbf{q} \rangle = \frac{1}{(\pi\sigma^2)^{N/4}} \exp \left[-\frac{(\mathbf{x} - \mathbf{q})^2}{2\sigma^2} + i \frac{\mathbf{p} \cdot (\mathbf{x} - \mathbf{q})}{2\hbar} \right]. \quad (2)$$

The problem is to find the value of the spatial spread of the wave packet, which is defined by the parameter σ .

At the same time, there has been interest in methods which allow the reduction of quantum calculations to classical ones, through the introduction of a suitable *effective potential*. The earliest known approach was provided by Wigner [17], where he introduced an expansion of the classical potential in powers of \hbar and $\beta = 1/k_B T$. This series leads to the well-known Wigner-Kirkwood expansion of the potential often used in solutions for the Wigner distribution function. However, the series has convergence problems in cases with sharp potentials, such as the Si-SiO₂ interface. Feynman [18] found a similar result, but also introduced a different approach, in which an effective potential is found from the free energy. For the case of a free particle, the exact variational minimization leads to a Gaussian weighting of the potential around the classical path, and this automatically includes quantum effects into the trajectory. Indeed, Feynman found that the smoothing parameter σ should have the value

$$\sigma^2 = \frac{\hbar^2}{12mk_B T}, \quad (3)$$

where λ_D is the thermal de Broglie wavelength. The connection of this to our earlier wave packet lies in the fact that the total Hamiltonian for a spatially varying potential involves weighting the potential at x by the density at this position. The Gaussian spread of the density is easily transformed into a Gaussian weighting of the potential [12], so that these approaches are consistent. The effective potential approach has been reviewed by Cuccoli *et al.* [19]. In Si, Eq. (3) gives a value of 0.52 nm for the value in the direction normal to the interface (at room temperature). A different mass would be used for transport along the channel, and this gives a value of 1.14 nm.

2.2 Device Simulation

The device structure is an n -channel SOI MOSFET, whose structure is shown in Fig. 2. The gate length is taken to be 40 nm including a 2 nm overlap of the uniformly-doped source and drain regions, which were each 50 nm in length. The device width was taken to have a relatively large value of 0.48 μm to provide smoother current calculations. The silicon film thickness was $T_{Si} = 5$ nm, the gate oxide $T_{ox} = 2$ nm, the buried oxide $T_{BOX} = 35$ nm, and the channel was doped uniformly at a level of $N_A = 5 \times 10^{17} \text{ cm}^{-3}$. In Fig. 3, we plot the potential in the device. The gradual decrease of the potential from the two oxides (the gate oxide and the buried oxide) is a result of the smoothing of the actual sharp potential by the Gaussian functions of Eq. (2). It is this smoother potential that leads to the size quantization in the channel and reflects this in the transport of the carriers.

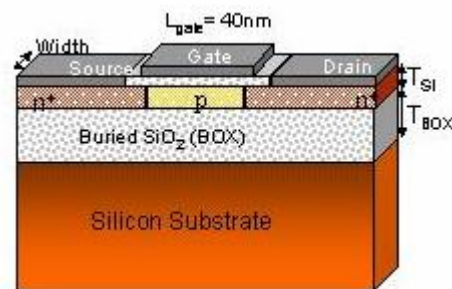


Figure 2. SOI MOSFET device schematic. The dimensions are discussed in the text.

Transport is treated by a standard ensemble Monte Carlo technique. In addition to surface roughness scattering, we have included acoustic phonon scattering, and optical phonon absorption and emission for the f and g , 0th and 1st

order processes. We include surface roughness as an additional scattering rate calculated for a given effective field, given by the normal approach, as:

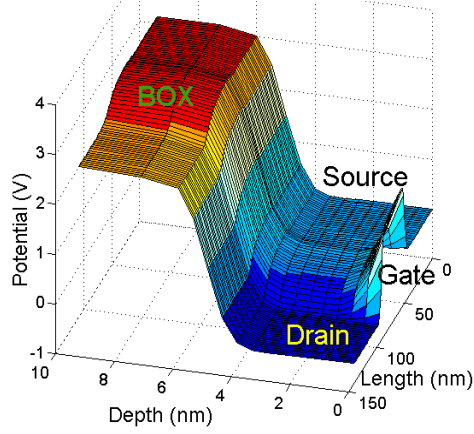


Figure 3. The smoothed effective potential for the SOI MOSFET, showing how the Gaussian smoothing takes out the sharp potentials at the oxide interfaces.

$$\Gamma(k) = \frac{m * (\Delta E_{avg} L e^2)^2}{2\hbar^3 \epsilon_s^2} \int_0^{2\pi} d\theta \frac{1}{(1 + k^2 L^2 \cos^2(\theta/2))^{1.5}}. \quad (4)$$

Here, we have used an exponential autocorrelation function to describe the surface roughness, as was detailed in [20]. The r.m.s. height of the surface roughness Δ is taken to be 0.48 nm, and the correlation length L is 1.3 nm. These values were found to provide good agreement to experimental mobility data. We calculate the average normal field using

$$E_{avg} = \frac{e}{\epsilon_s} (N_{depl} + 0.5n_s), \quad (5)$$

where N_{depl} and n_s are the areal depletion and inversion densities.

Figure 4 shows the results of the I_D - V_G simulations with an applied drain bias of 0.1 V. The simulations including the effective potential show the characteristic shift towards higher threshold voltage that is typical when including quantum effects. The I_D - V_D characteristics for the device are shown in Figure 5 for a gate bias of 0.3 V, which was the bias observed in Fig. 4 to be the point where surface roughness scattering was becoming appreciable. As expected, the surface roughness scattering tends to decrease the drive current in

saturation for both the classical and effective potential simulations. The classical simulations tend to have more charge in the channel at a given gate voltage, which results in increased surface roughness scattering.

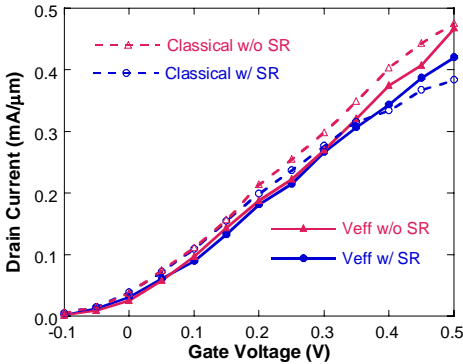


Figure 4. I_D - V_G behavior of the SOI MOSFET for simulations performed classically or with the effective potential and with or without surface roughness scattering.

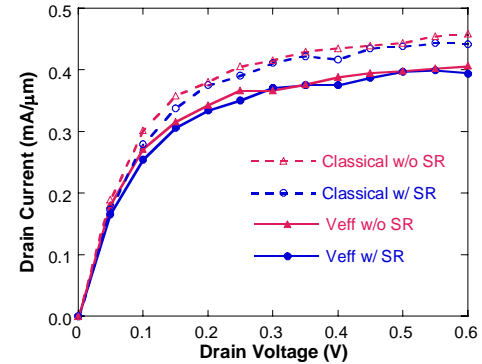


Figure 5. I_D - V_D characteristics for the SOI MOSFET with a gate bias of 0.3 V.

3. Quantum Transport with the Wigner Function

As EMC relies on the particle nature of the electron, quantum effects associated with the wave-like nature of the electron are difficult to fully incorporated into the simulation. In order to resolve quantum mechanical effects, the wave-like nature of the electron needs to be incorporated into the EMC. One first approach was via the effective potential discussed in the previous section, but this does not account for quantum interference. Hence, attention often is turned to the quantum mechanical Wigner distribution function (WDF), which has

found success in modeling resonant tunneling diodes (RTD) [21-23]. The similarities between BTT and the Wigner transport equation (WTE) [2,24], along with the fact that both utilize localized distributions, naturally leads to the conclusion that EMC should be a valid method for solving the WTE. The main difference between the BTE and the WTE is the non-local potential term of the WTE, which differs from BTT by treating the potential term non-locally (and fully incorporates quantum effects such as tunneling and correlation). This can cause the WDF to have negative parts. Unlike BTT, the WDF is not a normal probability function in that it can have negative values (negative probabilities have been discussed by Feynman [25]). An additional difference between direct solutions of the WTE and EMC solutions of BTT is that, although the physics that governs scattering in both transport equations is identical, incorporating scattering into the WTE is not an easy process and has not yet been fully achieved. Hence, the two major tasks are to augment the Monte Carlo procedure to account for negative probabilities and to incorporate quantum nonlocal scattering.

3.1 The Particle Affinity

To account for negative parts of the WDF, we assign the particles a new property termed the *affinity* [26]. The affinity is a weight given to each particle that represents its contribution to the total charge distribution of the system. The magnitude of the affinity is limited to ≤ 1 , but it can take on negative values to account for negative probabilities. By using Monte Carlo techniques to solve the WTE, augmented with the particle affinity, it is possible to incorporate quantum effects, such as tunneling, into a method previously unable to demonstrate such physical processes. The WTE is given by

$$\frac{df_w(x, k, t)}{dt} + \mathbf{v} \frac{df_w(x, k, t)}{dx} - \theta[f_w(x, k, t)] = \frac{df_w(x, k, t)}{dt} \Big|_{collision}, \quad (6)$$

where the last term accounts for scattering, the second term is the “diffusive” term and the third term incorporates the potential in the system, and is given by

$$\theta[f_w(x, k, t)] = \frac{1}{2\pi\hbar} \int dk' W(x, k') f(x, k + k', t), \quad (7a)$$

where the kernel is

$$W(x, k') = \int dx' \sin(k'x') \left[V\left(x + \frac{x'}{2}\right) - V\left(x - \frac{x'}{2}\right) \right]. \quad (7b)$$

As V in Eq. (7b) is the total potential, which includes both the barrier and the self-consistent potentials, calculating such a kernel has to be continuously updated since the self-consistent potential is dynamic. This is a computational problem. If the potential is second order or less, Eq. (7) reduces to [27]

$$\theta[f_w(x, k, t)] = \frac{1}{\hbar} \frac{dV(x)}{dx} \frac{df(x, k, t)}{dk}, \quad (8)$$

which is the classical force term of BTT. As the self-consistent potential is slowly varying, it is possible to decouple it from the barrier potential. Hence, barrier potentials, which are static, are treated using Eq. (7) while the self-consistent potential is included using Eq. (8). The final equation is

$$\begin{aligned} \frac{df_w(x, k, t)}{dt} + \mathbf{v} \cdot \frac{df_w(x, k, t)}{dx} \\ - \frac{1}{\hbar} \frac{dV(x)}{dx} \frac{df(x, k, t)}{dk} - \theta[f_w(x, k, t)] = \frac{df_w(x, k, t)}{dt} \Big|_{collision} \end{aligned} \quad (9)$$

The first three terms of Eq. (9), together with the scattering term, are BTT. The last term on the left-hand side is the quantum Wigner potential.

Two systems are now solved simultaneously. The first is the particle system, which resembles a standard EMC. That is, all particles in the system are treated classically as whole particles, and are scattered, drifted, and accelerated using the standard terms. Once the above operations have completed, the Wigner distribution function is calculated from the particle's position and affinity according to

$$f_w(x, k) = \sum_i \delta(x - x_i) \delta(k - k_i) A(i), \quad (10)$$

where k_i , x_i and $A(i)$ are the momentum, position and affinity, respectively, of the i^{th} particle. By constructing the distribution function, we then utilize Eq. (7) to calculate the non-local Wigner potential, which determines the change of the affinity that each particle experiences due to the quantum structure in the system. In this sense, the "particles" themselves do not see the quantum barriers, only their affinities "see" the barrier.

We are able to utilize full ensemble statistics by noting that any ensemble average takes the form

$$\langle Q \rangle = \frac{\sum_i A(i) Q(i)}{\sum_i A(i)}, \quad (11)$$

where Q is the quantity of interest. If we set the particle affinity to 1 (i.e. a classical EMC), we regain the well-known definition of the ensemble. The total number of electrons in the system is therefore given as

$$N = \sum_i A(i). \quad (12)$$

Because some $A(i) < 0$, we require the number of simulated particles to be much larger than the number of electrons. To achieve this, we define a maximal envelope (ME), which is a larger particle distribution. Here, the ME at any phase point is larger than the magnitude of f_w , as if all $A(i) = 1$. The electron density is then spread physically over the ME ensuring that no one particle contributes more than 1 electron to the distribution. The importance of using the ME is to ensure that enough particles are present not only to gain and lose affinity due to the NLP, but also to sample the entire phase-space of the WDF. In Fig. 6, we plot the tunneling of a Gaussian wave packet through a single 3 nm, 0.3 eV barrier. Clearly observable are the reflected and transmitted parts, as well as the correlation that remains in the barrier region. The total wave function is termed a macroscopic quantum superposition [28].

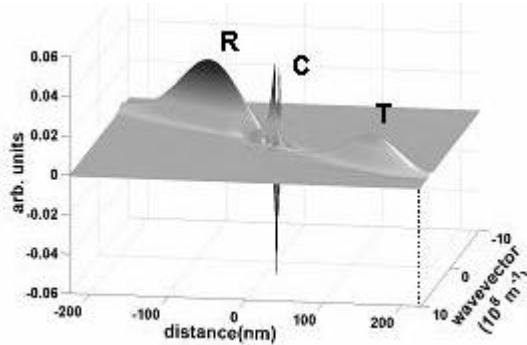


Figure 6. The Wigner distribution function for the correlation (C), transmitted (T), and reflected (R) wave packets.

We then simulate a 1-D (in space) RTD which consists of 3 nm, 0.3 eV barriers surrounding a 5 nm quantum well. The barrier structure is centered in a 30 nm lightly-doped (10^{16} cm^{-3}) spacer region connected to 60 nm highly-doped (10^{18} cm^{-3}) drift regions on either side. The device is considered to be entirely GaAs ($m^* = 0.067$), which is degenerate at these doping levels. Full Fermi-Dirac statistics are used in the calculation, which is performed at 300 K. Polar optical scattering, with both absorption and emission terms, is included using

standard EMC techniques. Self-consistency is included by solving the Poisson equation by a direct matrix inversion. Each bias point reaches steady-state within 2 ps. The resulting I-V characteristics are shown in Fig. 7. It is evident from this I-V characteristic that the method predicts the negative differential resistance expected in this device. Furthermore, the peak and valley locations are approximately where expected.

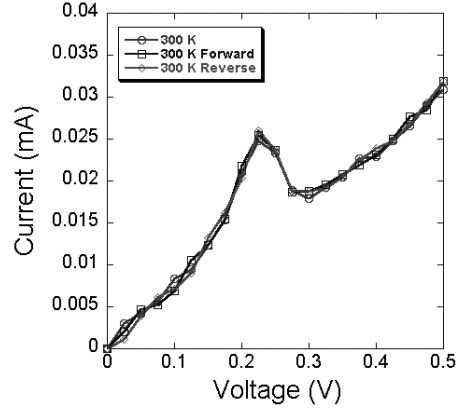


Figure 7. Current voltage characteristics achieved by initially increases the bias from 0–0.5 V and then reducing the bias stepwise back to 0 V. An additional forward bias run is also included to demonstrate that small differences in the currents are due to EMC noise.

3.2 Nonlocal Scattering

To treat non-local scattering, we need to account for two effects: (1) the collision duration and (2) the position change during the collision. The collision duration is the time required to build up correlation between the initial and final states and to then destroy this correlation once the collision has completed. This is typically a few femtoseconds [29,30], and is exponentially distributed [31,32]. We generate the collision duration by a random number, chosen by

$$\tau_e = -\tau_{coll} \ln(r), \quad (13)$$

where r is a random number and τ_{coll} is the mean collision duration time, which is of the order 1-3 fs [29].

The change in position is a direct result of the collision duration, as it is a displacement of the final state by

$$x_0 = v\tau_e + \frac{eF}{m^*} \frac{\tau_e^2}{2}, \quad (14)$$

where F is the electric field the electron experiences during the collision duration (the intra-collisional field effect). However, the interaction between the initial and final electron wave functions satisfies an overlap integral

$$I(x, x_0) = \int \Psi_i^*(x) \Psi_f(x + x_0) dx. \quad (15)$$

where x_0 is given by Eq. (14). Using the Gaussian wave of Eq. (2), this is

$$I(x, x_0) = \frac{1}{2\pi\sigma^2} \int e^{-\frac{x^2}{2\sigma^2}} e^{-\frac{(x-x_0)^2}{2\sigma^2}} dx \rightarrow \frac{1}{\sqrt{4\pi\sigma^2}} e^{-\frac{x_0^2}{4\sigma^2}}, \quad (16)$$

where σ is 1.9 nm in GaAs. The probability density for the particle being displaced by x_0 is then given by the square of the last term in Eq. (16). As the displacement becomes large, the probability of finding a final state for the electron decreases. This probability is used to determine whether the event occurs or not via a rejection technique.

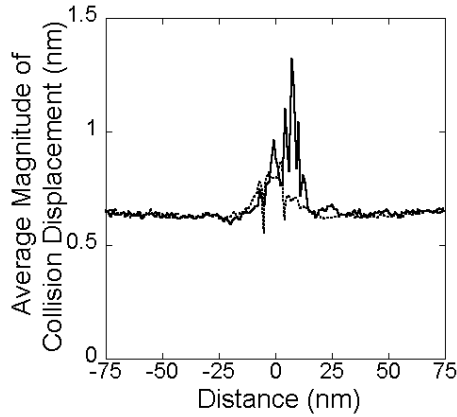


Figure 8. Average magnitude of the collision displacement during scattering vs. the position in the device. The solid line is for a bias of 0.0 V and the dashed line is for a bias of 0.5 V.

We conserve the total energy during the scattering process (see Fig. 1), which leads to

$$E_{p\pm q} = E_p \pm \hbar\omega_0 + V(x) - V(x + x_0). \quad (17)$$

In Fig. 8, we plot the average magnitude of the collision displacement as a function of position in the RTD for 0 and 0.5 V applied bias. In the emitter and collector regions, the average displacement is 0.6 nm, which corresponds to a thermal velocity, but still is smaller than σ . At zero bias, an increase in the

displacement in the barrier region occurs due to the presence of a large electric field of the barrier. The displacement then decreases due to lower electron energies in the well, and then again increases as electrons move into the well and sense the barrier. As the device potential is symmetric in this case, the curve then repeats. At 0.5 V, we see a large increase in the displacement downstream of the barrier. This is caused by the large bias that is applied, which creates a rapidly decreasing potential across the barrier region, therefore subjecting electrons to larger fields. It is clear that the ICFE only occurs in the presence of large electric fields, hence is observed primarily in this downstream region near the barrier.

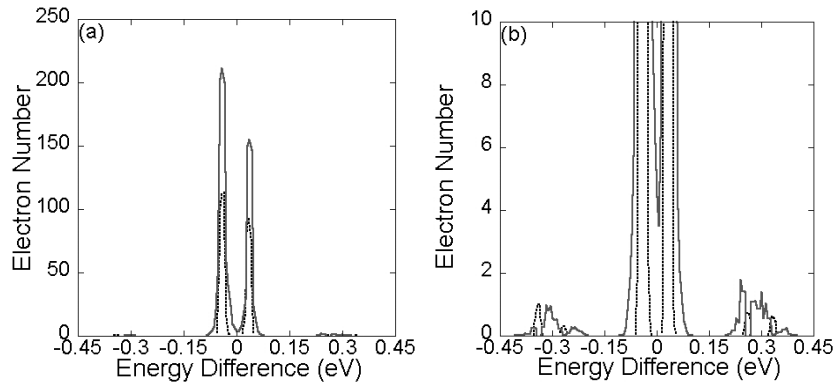


Figure 9. (a) The electron number sampled over 2 ps in the barrier region of the RTD is plotted versus the energy change experienced during phonon scattering. (b) “zoom” of Figure 2 (a) to resolve finer details occurring around the barrier energy.

In Fig. 9(a), we plot the number of scattering events in the region of the quantum barriers, as a function of the energy change experienced by these electrons (negative corresponds to emission of polar optical phonons). Classically, delta functions are expected at the phonon energy. However, we see broadened functions. The broadening increases with larger bias, which is expected due to electrons interacting with the fields in the system. Electrons are allowed to scatter (by either absorption or emission) from low potential regions onto the barriers and vice versa, which is visible in the magnification in Fig. 9(b). It is clear that this effect is small, but does occur as expected.

4. Some Concerns on Irreversibility

There has been considerable interest in recent years, particularly in the Green's function community, in using integration paths that return to the initial time. In some sense, this assumes that the functions retain a full memory of the initial time, so that these paths exist. In fact, this isn't the case in systems where phase breaking destroys this memory. We illustrate this for the density matrix. The system of interest can be separated from the environment through the use of a projection operator [33,34], with the result that the reduced density matrix can be written as [35]

$$\begin{aligned} \frac{d\rho_S(t)}{dt} = & -i \left[\mathbf{L}_{11}(t) - \mathbf{L}_{12}(t) \mathbf{K}_{22}^{-1}(t) \mathbf{K}_{21}(t) \right] \rho_S(t) \\ & + i \sqrt{d_E} \mathbf{L}_{12}(t) \mathbf{K}_{22}^{-1}(t) \mathbf{H}_{22}(t,0) \rho_2(0) \end{aligned} \quad (18)$$

where the derivation depends upon the existence of the time-reversed operator

$$\begin{aligned} H(t, t') = & T^c \exp \left(-i \int_{t'}^t ds Q_D L(s) Q_D \right), \\ G(t', t) = & T^a \exp \left(i \int_{t'}^t ds L(s) \right), \end{aligned} \quad (19)$$

and

$$K(t) \equiv 1 + i \int_0^t dt' H(t, t') Q_D L(t') P_D G(t, t') \quad (20)$$

where $L(t)$ is the original Hamiltonian super-operator. Reversibility requires the existence of $\mathbf{K}_{22}^{-1}(t)$, which is not guaranteed. In fact, in the far-from-equilibrium steady state, the right-hand side of

$$\begin{aligned} \frac{d\rho_S(t)}{dt} = & -i \left[\mathbf{L}_{11}(t) - \mathbf{L}_{12}(t) \mathbf{K}_{22}^{-1}(t) \mathbf{K}_{21}(t) \right] \rho_S(t) \\ & + i \sqrt{d_E} \mathbf{L}_{12}(t) \mathbf{K}_{22}^{-1}(t) \mathbf{H}_{22}(t,0) \rho_2(0). \end{aligned} \quad (21)$$

must vanish. Since this must occur regardless of the initial state, there is no unique initial state once the steady state have been achieved and no unique integration path back to the initial state.

References

1. D. K. Ferry and J. R. Barker, *VLSI Design* **8**, 165 (1998).

2. D. K. Ferry and H. L. Grubin, in *Solid State Physics* **49**, 283 (1995).
3. See, e.g., R. Zwanzig, *Phys. Rev.* **124**, 983 (1961).
4. R. Lake and S. Datta, *Phys. Rev. B* **45**, 6670 (1992).
5. P. Lugli and D. K. Ferry, *Phys. Rev. Lett.* **56**, 1295 (1986).
6. R. P. Joshi and D. K. Ferry, *Phys. Rev. B* **43**, 9734 (1991).
7. D. K. Ferry, A. M. Kriman, H. Hida, and S. Yamaguchi, *Phys. Rev. Lett.* **67**, 633 (1991).
8. See, e.g., J. R. Barker, *Sol.-State Electron.* **21**, 267 (1978).
9. D. K. Ferry and H. L. Grubin, *Proc. IWCE-6, Osaka* (IEEE Press, New York, 1998) pp. 84-7.
10. D. Vasileska *et al.*, *IEEE Trans. Electron Dev.* **44**, 577 (1997); **44**, 584 (1997).
11. J. R. Zhou and D. K. Ferry, *IEEE Trans. Electron Dev.* **39**, 473 (1992).
12. D. K. Ferry, *Superlatt. Microstruc.* **27**, 59 (2000).
13. See, e.g., R. T. Skodje *et al.*, *Phys. Rev. A* **40**, 2894 (1989), and references therein.
14. R. J. Glauber, *Phys. Rev.* **131**, 2766 (1963).
15. J. R. Klauder, *J. Math. Phys.* **4**, 1055 (1963); **4**, 1058 (1963); **5**, 177 (1964).
16. J. R. Klauder and E. C. G. Sudarshan, *Fundamentals of Quantum Optics* (Benjamin, New York, 1968).
17. E. P. Wigner, *Phys. Rev.* **40**, 749 (1932).
18. R. P. Feynman and A. R. Hibbs, *Quantum Mechanics and Path Integrals* (McGraw-Hill, New York, 1965).
19. A. Cuccoli *et al.*, *Phys. Rev. B* **45**, 2088 (1992).
20. S.M. Goodnick *et al.*, *Phys. Rev. B.* **32**, 8171 (1985).
21. U. Ravaoli *et al.*, *Physica B + C* **134B**, 36 (1985).
22. W. R. Frensley, *Phys. Rev. B.* **36**, 1570 (1987).
23. N. C. Kluksdahl *et al.*, *Phys. Rev. B* **39**, 7720 (1989).
24. E. Wigner, *Phys. Rev.* **40**, 749 (1932).
25. Feynman, R., in *Quantum Implications, Essays in Honour of David Bohm*, B. J. Hiley and F. D. Peat, Eds. (Routledge & Kegan Paul, London, 1987) pp. 235-248.
26. L. Shifren and D.K. Ferry, *Phys. Lett.* **A285**, 217 (2001).
27. C. Jacoboni *et al.*, *Math. Comp. Simul.* **55**, 67 (2001).
28. R. B. Griffiths, *Consistent quantum theory* (Cambridge University Press, Cambridge, 2002) pp. 134-136.
29. P. Bordone, D. Vasileska, and D. K. Ferry, *Phys. Rev. B* **53**, 386 (1996).
30. P. Lipavsky, F. S. Khan, A. Kavlova, and J. W. Wilkins, *Phys. Rev. B* **43**, 6650 (1991).
31. D. K. Ferry, A. M. Kriman, H. Hida, and S. Yamaguchi, *Phys. Rev. Lett.* **67**, 633 (1991).
32. P. Bordone, D. Vasileska, and D. K. Ferry, in *Hot Carriers in Semiconductors*, Ed. By K. Hess *et al.* (Plenum, New York, 1996) 433.
33. R. Zwanzig, *J. Chem. Phys.* **33**, 1338 (1960).
34. H. Mori, *Prog. Theor. Phys.* **33**, 423 (1965).
35. I. Knezevic and D. K. Ferry, *Phys. Rev. E*, in press.